

Journal Pre-proof

The coalescence of incipient soot clusters

Akaash Sharma, Khaled Mosharraf Mukut, Somesh P. Roy, Eirini Goudeli

PII: S0008-6223(21)00448-6

DOI: <https://doi.org/10.1016/j.carbon.2021.04.065>

Reference: CARBON 16274

To appear in: *Carbon*

Received Date: 3 February 2021

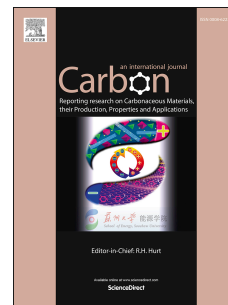
Revised Date: 16 April 2021

Accepted Date: 19 April 2021

Please cite this article as: A. Sharma, K.M. Mukut, S.P. Roy, E. Goudeli, The coalescence of incipient soot clusters, *Carbon*, <https://doi.org/10.1016/j.carbon.2021.04.065>.

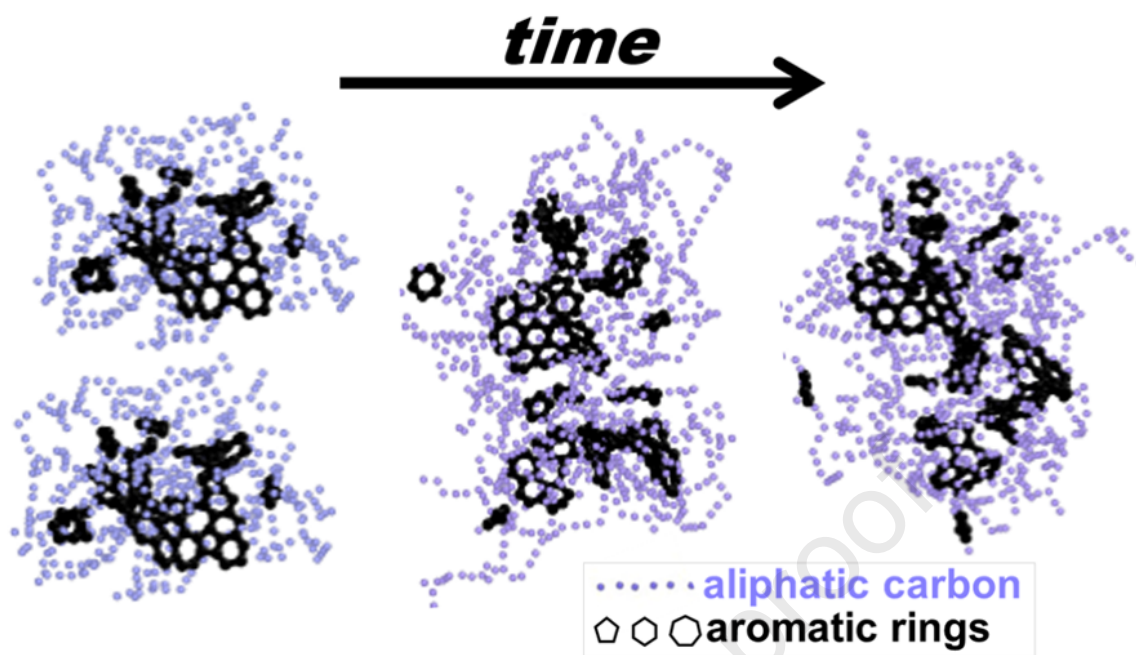
This is a PDF file of an article that has undergone enhancements after acceptance, such as the addition of a cover page and metadata, and formatting for readability, but it is not yet the definitive version of record. This version will undergo additional copyediting, typesetting and review before it is published in its final form, but we are providing this version to give early visibility of the article. Please note that, during the production process, errors may be discovered which could affect the content, and all legal disclaimers that apply to the journal pertain.

© 2021 Elsevier Ltd. All rights reserved.



Author contributions

Akaash Sharma: Methodology, Software, Visualization, Writing - Review and Editing. **Khaled Mosharraf Mukut:** Methodology, Software, Visualization, Writing - Review and Editing. **Somesh P. Roy:** Methodology, Writing - Original Draft, Writing - Review and Editing, Supervision. **Eirini Goudeli:** Methodology, Writing - Original Draft, Writing - Review and Editing, Supervision, Conceptualization.



The coalescence of incipient soot clusters

Akaash Sharma¹, Khaled Mosharraf Mukut², Somesh P. Roy² and Eirini Goudeli^{1,}*

1. Laboratory of Aerosol and Particle Technology, Department of Chemical Engineering, The University of Melbourne, Parkville, Melbourne VIC, Australia.

2. Department of Mechanical Engineering, Marquette University, Milwaukee, WI, USA.

Ph. +61 (0) 3 8344 5798

Submitted to:

Carbon

February 3, 2021

and revised on:

April 16, 2021

*Corresponding author: eirini.goudeli@unimelb.edu.au

Abstract

Reactive molecular dynamics (MD) simulations are employed to investigate the coalescence of incipient soot clusters. Initially, one thousand acetylene molecules collide and react with each other, allowing bond breakage and new bond formation upon collision, leading to various species (e.g., linear hydrocarbons, branched polyaromatic hydrocarbons) up to the formation of nascent soot clusters with diameter of up to 3.5 nm. The structure and composition of the formed soot clusters are quantified by the packing density and carbon-to-hydrogen (C/H) ratio, respectively, during nucleation and up to the formation of large nascent soot nanoparticles. Then, the nucleated incipient soot clusters are isolated from the surrounding reactive species and are allowed to coalesce with each other isothermally to investigate soot coalescence. The coalescence between incipient soot clusters of different sizes is elucidated at various process temperatures, ranging from 800 to 1800 K. The characteristic coalescence time of nascent soot is quantified by tracking the evolution of the particle surface area, for the first time. Soot clusters consisting of up to 760 atoms coalesce instantly (within 0.1 ns), especially at relatively low temperatures (i.e., 800 – 1000 K). At higher temperatures (1200 – 1600 K), incipient soot clusters are less prone to coalescence due to the larger fraction of constituent aromatic rings leading to more rigid particles. Large clusters consisting of more than 1300 atoms do not coalesce within the time scales investigated here (i.e., up to 5 ns). The employed reactive MD approach gives significant insight into fundamental soot formation and growth mechanisms, which are typically treated semi-empirically, facilitating a better understanding and more efficient control of soot in combustion processes.

Keywords: incipient soot, nucleation, coalescence, reactive molecular dynamics

1. Introduction

Soot clusters are undesired carbonaceous nanoparticles formed during incomplete combustion of hydrocarbon fuels¹. These carbonaceous nanoparticles are emitted from combustion sources, such as combustion engines, diesel vehicles in urban environments and coal burning for power generation, or biomass burning, such as wildfires. Such particles (soot) have adverse effects on public health and atmospheric pollution. For example, exposure to soot and particulate matter can cause DNA mutations, lung cancers² and cardiovascular diseases³. In addition, soot particles act as nuclei for ice formation, affect cloud properties such as their lifetime, emissivity and albedo⁴ and, when associated with non-absorbing aerosols constituents, like sulfate, they increase the positive radiative forcing nearly balancing the net cooling effect of other anthropogenic aerosols⁵. Yet, some forms of carbonaceous nanoparticles are reproducibly generated in materials science in the form of carbon black, the largest flame-made nanostructured material by volume and value since the early 2000s^{6,7}. These carbon-based engineered particles find niche market applications, including catalysis (e.g., carbon-coated cobalt nanoparticles can be used as organocatalysts that can be recycled by rapid magnetic separation⁸), energy harvesting applications (e.g., carbon nanotubes combined with fluoropolymers exhibit high piezoelectric activity⁹) or bioimaging (e.g., carbon-based quantum dots have great potential as fluorescent labels for cellular imaging¹⁰).

Due to the enormous complexity of the reaction networks involved in combustion, major complications arise in modelling the kinetics of particle growth. The current understanding of soot formation broadly includes:¹¹ (a) formation of soot precursors and polycyclic aromatic hydrocarbons (PAHs), (b) inception of nascent soot from large PAHs, (c) surface growth by addition of gas-phase molecules, (d) particle agglomeration by coagulation, and (e) oxidation. The first stage of the formation of soot is nucleation or inception. In general, PAHs are believed to play a major role as soot precursors¹¹. The details of soot formation have been subject of debate over the years. The coalescence, stacking and dimerization of PAHs (e.g., pyrene,¹² coronene¹³) is the most commonly adopted nucleation mechanism in currently available detailed soot models, supported by experiments¹¹. However, recent reactive molecular dynamics (MD) simulations,¹⁴ electronic structure calculations¹⁵ and vacuum ultraviolet aerosol mass spectrometer measurements¹⁵ indicated that PAH dimerization hardly contributes to nucleation of soot, implying that other possible chemical pathways may lead to soot. Molecular dynamics simulations have been applied to combustion processes involving the formation of incipient soot particles by physical nucleation of pyrene and coronene,¹⁶ peri-condensed aromatics and PAHs with aliphatic chains^{17,18} or by chemical nucleation¹⁹ owing to

the development of reactive forcefields. However, most of those computational studies are limited to the homomolecular dimerization rates of a limited number of PAHs that have been traditionally believed to contribute to incipient soot formation, neglecting the effect of radicals or other soot precursors. Soot formation accounting for chemical reactions has also been studied by nucleation of oxygenated compounds during diesel combustion at 3000 K²⁰ or of heterogeneous PAHs in the presence of small reactive species at 1000 – 1750 K²¹, leading to the formation of aromatic-aliphatic linked hydrocarbons.

Once formed, the nascent soot particles evolve due to physical or chemical interactions such as agglomeration, aggregation and chemical reactions with gas-phase species such as adsorption and/or condensation of PAHs.²² During soot growth, the coalescence among soot clusters (sometimes ambiguously referred as “sintering” in a nod to inorganic nanoparticle terminology¹) can lead to particle restructuring and surface area reduction. However, coalescence is typically either neglected or simplified in detailed soot models. Recent scanning mobility particle size²³ and primary particle size distribution measurements²⁴ support that coalescence of soot primary particles can take place in the inception flame region and becomes less important at higher heights above the burner.²⁴ Monitoring the soot particle size distribution by transmission electron microscopy (TEM) image counting as function of the height above the burner showed²⁴ that the particle size distributions shift to smaller particle sizes and narrow down, indicating particle coalescence.

In metallic nanoparticles, sintering (a process similar to coalescence in soot) depends on particle size, process temperature and even crystallinity, as shown by MD simulations of gold nanoparticles²⁵. Non-reactive MD simulations have been used to study the coalescence of soot particles consisting of stacked homogeneous PAHs exhibiting rapid coalescence at temperatures higher than the clusters’ melting point with characteristic coalescence times, τ_c , at the order of 0.01 ns and slower coalescence ($\tau_c \approx 5$ ns) at lower temperatures ($T \lesssim 500$ K)²⁶. Nonetheless, such non-reactive simulations do not account for new chemical bond formation or breakage that might take place between the coalescing species.

Here, incipient soot formation and coalescence is investigated *in silico* by reactive MD simulations, for the first time, without making *a priori* assumptions about the soot cluster constituent building blocks. The base configuration resembles with soot formation in acetylene pyrolysis. Nascent soot clusters with diameter of up to 3.5 nm are formed by clustering reactions of acetylene molecules at 1500 K. The atomic composition and structural characteristics of the formed nascent soot particles are quantified by the C/H ratio, packing density, aliphatic-to-

aromatic ratio and the number of 5-, 6- and 7-member rings. These incipient soot clusters are then extracted and placed next to each other in vacuum to allow their coalescence. The characteristic coalescence time of pairs of equally sized soot clusters adhering to each other with random initial orientations is calculated by tracing the evolution of the total surface area during particle coalescence²⁷. The probability of coalescence is determined for various particle sizes as function of temperature.

The novelty of this work lies in exploring the formation and growth of the soot clusters from pure acetylene without making any a priori assumption about possible pathways to soot or the characteristics of soot itself. This work provides an important glimpse at the inception of soot and coalescence of incipient soot clusters and can facilitate the design of more energy-efficient, soot-free and selective chemical processes.

2. Theory

2.1 Molecular Dynamics (MD)

One thousand acetylene molecules are randomly distributed in a simulation cell with dimensions of $83 \times 68 \times 74 \text{ \AA}$, corresponding to acetylene density of 0.1 g/cm^3 . A density higher than realistic flame conditions is used to ensure that nucleation and incipient soot cluster formation takes place within a few nanoseconds. Previous studies²⁸ of acetylene reactions by reactive MD simulations have shown that the initial acetylene density does not affect the mechanism of carbon black formation. Acetylene molecules react at 1500 K, a temperature relevant for soot formation in combustion environment,²⁹ accounting for bond breakage and new bond formation upon molecular collisions by employing the reactive force field (ReaxFF) of Castro-Marciano et al.³⁰ for hydrocarbons. In ReaxFF the bond lengths are adjusted based on changes in the local chemical environment and are updated at every MD step³¹. Therefore, bond cleavage and bond formation are described accurately during chemical reactions leading to the formation of radicals in the nucleation stage of soot. The equations of motion are integrated by the velocity-Verlet algorithm³² with a timestep of 0.25 fs ³³ using the Nosé-Hoover thermostat³⁴ with a damping parameter of 10 fs. The simulations are performed in the NVT (constant number, volume and temperature) ensemble for up to 10 ns using the LAMMPS³⁵ MD code.

2.2 Extraction of incipient soot clusters

Soot clusters are isolated from the surrounding molecules at various stages of soot inception at 1500 K and are simulated isothermally in the *NVT* ensemble in vacuum at different temperatures ranging from 800 to 1800 K for up to 0.5 ns. The rationale of the single-particle isothermal simulations is to emulate the physicochemical restructuring of soot clusters during thermal aging. During cluster restructuring, atoms or small molecules (of up to 3% of the initial number of atoms) leave the particle surface without practically altering the particle size.

2.3 Characteristic coalescence time

Pairs of particles with random initial orientations are placed next to each other at a minimum separation distance of 0.3 nm³⁶ in a cubic simulation cell with dimensions 300 × 300 × 300 Å, applying non-periodic boundary conditions.²⁵ The separation distance of 0.3 nm is chosen to ensure that the closest atoms between the two coalescing clusters are close enough to ensure instant adhesion. Once particles are placed close to each other, they adhere either by reactions forming new chemical bonds or by weak non-bonded interactions. Upon adhesion, the particles either stick and fuse or they dissociate. The evolution of the surface area of particles that stick is determined using the MSMS 6.2.1³⁷ code, which calculates the solvent-accessible area (free surface area) of overlapping spheres. A probe radius of 2.25 Å is employed for the surface area calculation, corresponding to that of a N₂ molecule. This method of surface area calculation is comparable to the measurement of the specific surface area by N₂ adsorption³⁸.

For each pair of particles, seven random initial orientations were simulated for up to 3 ns at each temperature. The characteristic coalescence time, τ_c , is the time required for the neck diameter to reach 83% of the initial particle diameter.³⁹ This time corresponds to 67% reduction of the excess particle surface area over that of a fully coalesced sphere, a_s . The rate of change of the surface area by coalescence is:⁴⁰

$$\frac{da}{dt} = -\frac{1}{\tau_c}(a - a_s) \quad (1)$$

Although soot coalescence is typically neglected or overlooked in the literature, some models accounted for soot coalescence in ethylene/air diffusion⁴¹ and premixed flames⁴². Specifically, Veshkini et al.⁴¹ used a sectional soot model to describe soot coalescence by employing a surface diffusion mechanism model developed for titania particles (by combining equations 6 and 7 from Kobata et al.³⁹):

$$\tau_c = 7.44 \cdot 10^{16} d_p^4 T \exp\left(\frac{258,000}{RT}\right) \quad (2)$$

where d_p (m) is the particle diameter, T (K) is the temperature and R is the gas constant. Chen et al.⁴² also used a viscous flow coalescence rate (based on the sintering rate of amorphous silica)⁴³ in soot population balance equation to account for soot particle coalescence:⁴²

$$\tau_c = 1.1 \cdot 10^{-14} d_p \exp\left(\frac{799,000}{RT} \left(1 - \frac{1.58 \cdot 10^{-9}}{d_p}\right)\right) \quad (3)$$

where d_p is in m and T in K.

2.4 Chemical structure of soot clusters

The chemical structure of soot clusters is extracted by post-processing the MD-obtained atom coordinates from trajectory files of each cluster using a Python script developed in-house⁴⁴ using a structure-conversion method for organic molecules⁴⁵. The tool detects the number of aromatic rings (i.e., 5-, 6- and 7-membered rings), the total number of aromatic and aliphatic carbon atoms, and the coordinates of both aromatic and aliphatic components. Due to the highly interconnected nature of the network of molecules, a divide and conquer algorithm⁴⁶ is developed.

Initially, the whole domain is divided into several overlapping sets of smaller subregions. The subregions can overlap with each other to eliminate the possibility of losing any information of interconnectivity at the intersection of subregions. Then, each of these subregions is analyzed and the relevant soot chemistry is extracted.

First, the ring structures in the clusters are extracted by generating an adjacency matrix based on the range of carbon-carbon bond distances (1.3 Å – 1.6 Å) obtained from MD simulations. The adjacency matrix is converted into several simply connected graphs⁴⁷. Each graph corresponds to a different network of carbons in the cluster. After separating the graphs, an efficient algorithm⁴⁸ is used to identify all elementary circuits in the graph based on the minimum spanning tree using the Kruskal algorithm⁴⁹. The closed circuits (rings) are detected using a depth-first search algorithm⁵⁰ and the 5-, 6- and 7-membered circuits, representing the aromatic rings in each of the molecules in the cluster, are quantified. Once the aromatic rings are obtained, the aliphatic carbon atoms are identified.

The atomic coordinates of the identified aromatic and aliphatic carbon atoms are converted from atomic connectivity to bond orders by applying general chemical rules and valency information⁴⁵. First, the bond orders are

assigned to each atomic pair using the atomic valences as input. Then, the degree of bond saturation is calculated using the aromatic connectivity information. The bond order is assigned by trial and error, and when the atoms in each aromatic connectivity network achieve appropriate valence states, the bond order assignment is terminated. Once all atoms are assigned with a bond order, the information is converted to a simplified molecular-input line-entry system (SMILES)⁵¹. Similar to the detection of the aromatic rings, the Kruskal algorithm⁴⁹ is used to detect ring closures, while the primary chains and branches are identified based on the depth-first search algorithm⁵⁰. The SMILES-generated chemical structures of the closed rings are visualized using the “RDKit” open-source cheminformatics interface⁵².

3. Results and discussion

3.1 Incipient soot formation

Incipient soot particles are formed by nucleation and surface growth of acetylene molecules (Sec. 2.1). The nucleation simulation is similar to acetylene pyrolysis as there are no oxygenated species present. Even though nucleation starts only with pure acetylene, ReaxFF allows for bond breakage and bond formation, resulting in a plethora of hydrocarbons (both aromatic and aliphatic) that, in turn, lead to the formation of soot. Figure 1 shows the evolution of gas-phase molecules and nascent soot clusters at (a) 0.05, (b) 0.3, (c) 0.4 and (d) 2.7 ns, formed by collisions of acetylene molecules at 1500 K. Aromatic and aliphatic carbon chains are depicted as black lines while hydrogen atoms are omitted for clarity. The formation of incipient soot takes place at three different stages: the formation of linear chains (Fig. 1a), the cyclization stage where the formation of aromatic rings is observed (Fig. 1b), and the particle growth by surface reactions with small radicals and molecules present in the surroundings (Fig. 1c and d).

Initially (for $t < 0.05$ ns), the reactant species consist mainly of acetylene molecules and small linear hydrocarbons (highlighted by red circling in Fig. 1a). These linear chains formed at the early stages of nucleation consist mainly of carbon atoms and, typically, are terminated by hydrogen atoms. At this timestep ($t = 0.05$ ns), there are several hydrocarbon molecules in the simulation domain, with molecular weight of up to about 347 g/mol (corresponding to 26 carbon atoms). Upon continuous collisions, the straight chains stick with small radicals and with each other to form branches that lead to formation of branched PAHs (e.g., highlighted by red circling in Fig. 1b). The branched PAHs grow further by condensation of gaseous species on a network of aromatic rings till the

formation of a large soot cluster (Fig. 1c, red encircling) that grows constantly by condensation of small free linear radicals on its surface (Fig. 1d, red encircling) till their depletion. The above soot formation mechanism exhibits the same growth stages with carbon black at 2500 – 3500 K, elucidated by reactive MD²⁸.

Figure 1

The largest soot cluster formed during the simulation of nucleation and surface growth (encircled particle in Fig. 1b – d) is isolated from the surrounding molecules at different stages of its growth and is characterized by determining its composition and structural characteristics. Table 1 shows exemplarily snapshots of the incipient soot clusters obtained during nucleation and surface growth at 1500 K (Fig. 1) at different stages of their growth ($t = 0.25 - 2$ ns). Aromatic carbon rings are depicted by black lines whereas aliphatic carbon branches are depicted as blue beads. The number of atoms, radius of gyration, r_g , aromatic-to-aliphatic carbon ratio and number of 5-, 6- and 7-member rings are listed for each cluster. At the early stages of soot formation ($t \leq 1$ ns), the aromatic-to-aliphatic C ratio is small indicating that the clusters consist mainly by aliphatic carbon chains that occupy the particle surface, while the core consists of small aromatic islands (each containing 1 – 15 rings) linked together by aliphatic branches consistent with earlier reactive MD simulations²¹. As the particles grow further ($t > 1$ ns), the surface-to-volume ratio decreases and the clusters are composed primarily of large aromatic islands and only a few aliphatic chains that decorate the surface, leading to larger aromatic-to-aliphatic C ratios. The composition of the aromatic islands is quantified by the number of 5-, 6- and 7-member rings. Initially ($t < 1$ ns), all three types of aromatic rings exist in the cluster but no clear trend is observed in the fraction of 5-, 6- or 7-member rings, as the soot clusters consist of a few small aromatic islands cross-linked with aliphatic chains, corresponding to aromatic-to-aliphatic C ratios smaller than 1. In larger incipient soot particles with aromatic-to-aliphatic C ratios greater than 1, the aromatic islands consist mostly of 6-member rings (~55%) and a smaller fraction of 5- (~25 – 30%) or 7-member rings (~15 – 20%), regardless of the constituent number of atoms or the aromatic-to-aliphatic C ratio. These results are consistent with TEM,⁵³ indicating that incipient soot nanoparticles exhibit an aromatic core and aliphatic shell structure.

Table 1

The carbon-to-hydrogen (C/H) ratio of these MD-derived incipient soot clusters is between 2 – 3 (Supplementary Information: Fig. S1), consistent with CHNSO elemental analysis in premixed methane and ethylene flames⁵⁴ and laser desorption ionization combined with mass spectrometry⁵⁵ and atomic force microscopy measurements⁵⁶ obtained for incipient and primary soot clusters with low molar mass, providing an indirect

validation of the present reactive MD simulations. For larger soot clusters ($MW > 1$ kg/mol), the C/H ratio lies between the C/H ratios of peri- and cata-condensed PAHs⁵⁷. The volume-equivalent diameter of the soot cluster is also in line with reported values of peri-condensed PAHs for small clusters (Supplementary Information: Fig. S2). In addition, the shape of the MD-obtained soot clusters is quantified by their packing density, θ , and “atomic” fractal dimension, D_f (Supplementary Information: Fig. S3). The packing density is typically used to quantify the porous structure of nascent soot particles, while the “atomic” D_f is used to quantify the sphericity and is equivalent to the mass fractal dimension of aggregates⁵⁸ – except for the fact that C and H atoms are used instead of primary particles to calculate the fractal dimension. Small incipient soot clusters with $MW < 10$ kg/mol are non-spherical as their surface is occupied by long aliphatic chains. These low molecular weight clusters exhibit $\theta < 0.6$, indicating their highly porous structure, and D_f ranging from 1.2 (chain-like clusters) to 2.7 (spherical-like clusters), indicating their large morphological variations. Larger particles ($MW > 10$ kg/mol), however, become less porous and more spherical exhibiting $\theta > 0.6$ and “atomic” $D_f = 2.4 - 2.8$, consistent with packing density estimations⁵⁹ based on the ratio of the effective to bulk soot density (Supplementary Information: Eqs. S1 – S3) and discrete element method models of nascent soot growth in ethylene flames⁶⁰, respectively. Even though the surface of those particles is still decorated with aliphatic chains, they hardly affect the particle morphology, especially for small surface-to-volume ratios. This is evidenced by high resolution TEM images of soot particles obtained in spark ignition flames⁶¹.

Eight soot clusters consisting of 50, 247, 348, 449, 760, 1404, 1769 and 1927 atoms were used to investigate the effect of temperature, cluster size, structure and composition on coalescence dynamics. These clusters are referred as clusters A – H, with A being the smaller one consisting of 50 atoms and H being the largest one consisting 1927 atoms. Table 2 shows the snapshots of the incipient soot clusters A – H, obtained during nucleation and surface growth at 1500 K (Fig. 1). The number of atoms, radius of gyration, r_g , aromatic-to-aliphatic C ratio and number of 5-, 6- and 7-member rings are listed for each cluster. These clusters are then simulated isothermally in the *NVT* ensemble in vacuum at various temperatures to allow particle restructuring due to temperature-dependent chemical reactions, as described in Section 2.2 section.

Table 2

Figure 2 shows the effect of temperature on aromatic-to-aliphatic carbon ratio as function of temperature for incipient soot particles D (circles), E (squares), G (triangles) and H (diamonds), after the single-particle isothermal simulations (see Section 2.2). The number of atoms represent the total number of atoms for the cluster

when they were extracted from the nucleation simulation (at 1500 K). The temperatures indicate the temperature at which these clusters restructured before coalescence. Small soot clusters consisting of 449 (cluster D) and 760 atoms (cluster E) have fewer aromatic islands occupying their core and more aliphatic chains decorating the surface (see also Table 2) compared to larger particles G and H (i.e., consisting of 1769 and 1927 atoms). Such small clusters increase their aromatic-to-aliphatic carbon ratio with increasing temperature due to aromatization reactions taking place at high temperatures, consistent with Dandajeh et al.⁶² Larger soot clusters, however, exhibit higher aromatic-to-aliphatic carbon ratios (≥ 1.5), which are less sensitive to temperature for the timescales investigated here. The MD-obtained results are consistent with the ratio of aromatic C-H and aliphatic C-H obtained by photoionization aerosol mass spectrometry⁶³ and micro-Fourier transform-infrared spectroscopy (FTIR) measurements⁶⁴ of soot particles with average diameter of 10 nm sampled from premixed ethylene flames. These flame-made carbonaceous nanoparticles age as they travel in the high-temperature regions of flames for longer times (of the order of microseconds) than the timescales simulated here.

Figure 2

3.2 Incipient soot coalescence

Clusters A – H are replicated with random initial orientations and are placed next to each other in vacuum with interparticle distance of $\sim 3 \text{ \AA}$ to coalesce at various temperatures. Among those clusters, only particles B – E exhibit reduction to their surface to a value lower than 67%, indicating coalescence³⁶. Small clusters (i.e., cluster A) bounce without adhering to each other while bigger clusters (i.e., clusters G and H), although they can adhere to each other, they coalesce only partially, leading to minor surface area reduction. The surface area evolution of pairs of clusters that adhere, coalesce and bounce are shown exemplarily in the Supplementary Information, Fig. S4.

Figure 3 shows snapshots of two equally sized incipient soot clusters, corresponding to cluster E in Table 2, with initial radius of gyration, $r_g = 1.23 \text{ nm}$, coalescing at (a) 800 K and (b) 1600 K. Aliphatic C atoms are shown with blue dots and 5-, 6- and 7-member rings are depicted as black rings, while H atoms are omitted (left columns). At low temperature ($T = 800 \text{ K}$), each particle consists of 760 atoms, having $C/H = 2.78$ ($C_{559}H_{201}$). Initially ($t = 0$), clusters at $T = 800 \text{ K}$ are placed next to each other with random initial orientation. As time proceeds, the clusters approach each other and re-orient ($t = 0.01 \text{ ns}$) until they adhere to each other ($t = 0.1 \text{ ns}$) due to reactions taking place among their aliphatic surface branches. The chemical reactions taking place between the coalescing clusters are monitored by the radial distribution function, which reveals that the nearest carbon-carbon neighbors between

the two clusters are at a distance within the triple carbon-carbon bond length, indicating that chemical reactions take place during coalescence. The free-moving branches at the cluster surface occupy the concave region formed around the neck leading to reduction of the surface area. At longer times ($t > 0.1$ ns), the clusters coalesce leading to the formation of a compact oval-like dimer at 0.7 ns, hardly altering their shape ($t = 1.2$ ns). During coalescence, only the free aliphatic branches participate in the neck formation and no clustering of the core aromatic islands is observed. A movie of the coalescence dynamics of clusters (E, E) at 800 K is also shown in the Supplementary Information, Video S1. However, larger incipient soot clusters, such as clusters G and H, do not coalesce significantly within the time scales investigated here, as they behave as rigid spheres due to the high fraction of aromatic C atoms (snapshots of clusters (G, G) and (H, H) coalescing at 800 K are shown in the Supplementary Information, Fig. S5 and a movie of the coalescence dynamics of clusters (G, G) at 800 K is shown in the Supplementary Information, Video S2).

At high $T = 1600$ K, each particle E has lost seven H atoms upon restructuring during single-cluster isothermal simulations (see Section 2.2), attaining $C/H = 2.86$ ($C_{559}H_{194}$), while its aromatic-to-aliphatic C ratio has increased from 0.37 at 800 K to 0.58 at 1600 K. Similar to 800 K, the two particles adhere to each other at $t = 0.1$ ns, however, the neck formed between the particles hardly grows as function of time and the dimer maintains its concave region.

In addition, Fig. 3 shows the temporal evolution of the chemical structure of ring closures (right columns) of the coalescing clusters (E, E) identified based on the structure-conversion method described in Section 2.4. Large PAH structures are seen throughout coalescence at both temperatures. In each such cluster, 6-membered rings are held together by 5- (highlighted yellow areas) and 7-membered rings (highlighted red areas), as shown exemplarily at $t = 1.2$ ns, indicating the importance of those rings as hypothesized in recent studies^{15,65}. Most of these structures are found more than once in each cluster. Initially ($t = 0$ ns), even though the clusters contain relatively large PAHs composed of up to 12 rings at both temperatures, the PAH size does not increase during coalescence at $T = 800$ K as PAHs do not react with each other and coalescence takes place solely due to chemical reactions among the aliphatic branches of the clusters. In contrast, chemical reactions among PAHs are observed at higher temperatures (i.e., $T = 1600$ K), leading to formation of larger PAH structures within the coalescing clusters at $t \geq 0.1$ ns.

Figure 3

Figure 4a shows the temporal evolution of the aromatic-to-aliphatic C ratio of coalescing clusters (E, E) at 800 K (black line) and 1600 K (red line), discussed in Figure 3. At 800 K, the aromatic-to-aliphatic C ratio of clusters (E, E) is ~ 0.26 and does not change during coalescence, indicating that no aromatization takes place. At 1600 K, however, the fraction of aromatic C atoms increases as more rings are formed, leading to the formation of larger PAH structures (as shown in Fig. 3b, $t \geq 0.1$ ns). The number of 5- (brown lines), 6- (blue lines) and 7-member rings (green lines) of coalescing clusters (E, E) are also shown at 800 K (Fig. 4b) and 1600 K (Fig. 4c). At $T = 800$ K (Fig. 4b) the 6- and 5-member rings are the dominant types of aromatic rings found in clusters (E, E), while about 13% of the identified aromatic rings are 7-membered. Even though the number of 5-, 6- and 7-member rings fluctuates, their average number does not alter during coalescence. Nonetheless, the aromatization that takes place at $T = 1600$ K leads to an increase to all three types of aromatic rings, while the number of 5-member rings is comparable to that of 6-member rings, highlighting their importance in the soot clusters formed by coalescence at high temperatures.

Figure 4

The degree of coalescence is quantified by monitoring the normalized surface area during coalescence of pairs of clusters. These simulations can lead to full or partial coalescence or bounce of the two particles. Coalescence and bounce events result in decreasing and increasing surface area of the soot cluster pairs, a , respectively. Figure 5 shows the temporal evolution of the coalescing soot clusters surface area, a , normalized by the initial surface area before particle adhesion, a_0 , during coalescence of soot clusters with (a) initial $r_g = 1.23$ nm (pairs of cluster E, denoted here as (E,E)) at 1600 K (red line), 1200 K (green lines), 1000 K (blue lines) and 800 K (black lines) and (b) particles (E, E) (black line), (D, D) (blue line) and (C, C) (green line) at 800 K. The lightly colored shaded areas represent the variability of multiple coalescence simulations with random initial cluster orientations. The initial cluster orientation can affect the evolution of the surface area reduction and, in turn, the characteristic coalescence rate, as clusters rotate to find energetically favorable contact points or surfaces (please see Supplementary Video S2), delaying cluster adhesion. Such cluster rotation has been observed also for gold⁶⁶ and titania²⁷ nanoparticles. The broken horizontal line at $a/a_0 = 0.863$ indicates the characteristic coalescence time, τ_c , which corresponds to the time required for the free surface area to decrease by 67%³⁶.

For soot clusters (E, E) (Fig. 5a), the average a/a_0 hardly changes for $t < 10^{-3}$ ns as the clusters re-orient without adhering to each other. Nonetheless, the presence of aliphatic branches attached at the particle surface

causes abrupt fluctuations in the free surface area. For $t > 10^{-3}$ ns, the normalized surface area decreases upon coalescence due to the formation and growth of a neck at the interface of the two clusters. The temporal evolution of a/a_0 follows the same trend for all coalescing clusters, regardless of temperature. However, for clusters coalescing at low temperature (i.e., at $T = 800$ K), the normalized surface area drops slightly faster than at higher temperatures. This delay in the coalescence rate with increasing temperature is in stark contrast to the temperature dependence of the characteristic sintering time of monometallic²⁵, bimetallic⁶⁷ or oxide³⁶ nanoparticles obtained by tracking the MD-derived normalized surface area. This difference can be attributed to the aliphatic chains at the soot clusters' surface contributing to coalescence, which are absent from metallic or oxide nanoparticles. Furthermore, high temperatures favor the formation of additional aromatic rings in the soot clusters leading to an increase in the aromatic-to-aliphatic ratio (Fig. 2). Therefore, the soot clusters become more rigid and less prone to coalescence with increasing temperature.

At $T = 800$ K (Fig. 5b), soot clusters have similar evolutions in their normalized surface area during coalescence. For all particles, a/a_0 drops below the threshold of $a/a_0 = 0.863$ early on (within a few nanoseconds), indicating that coalescence is instant. Yet, the coalescence rate exhibits minor dependence on the soot cluster size: pairs consisting of larger clusters i.e., pairs (D, D) and (E, E), originally consisting of 449 and 760 atoms, respectively, at 1500 K during nucleation (Table 2), coalesce more slowly than pairs (C, C) consisting of clusters with 247 atoms each.

Figure 5

Figure 6a shows the MD-obtained characteristic coalescence time, τ_c (symbols), for coalescing incipient soot cluster pairs (B, B) (diamonds), (C, C) (triangles), (D, D) (circles) and (E, E) (squares) as function of the process temperature, T . The error bars show the minimum and maximum values of the coalescence rate obtained from up to seven coalescence simulations. As temperature increases, τ_c slightly increases for all cluster sizes, corresponding to slower coalescence. All cluster sizes, however, exhibit almost identical τ_c of ~ 0.1 ns (with a variation of two orders of magnitude) for the size ranges investigated here ($r_g = 0.81 - 1.23$ nm). The reactive MD-obtained τ_c is consistent with classic MD coalescence simulations of soot particles consisting of homogeneous PAHs exhibiting $\tau_c \approx 0.01$ ns at temperatures higher than their melting point²⁶. It should be noted, however, that classic MD coalescence simulations do not account for the dynamic evolution of soot composition and structural changes induced by reactions, but account only for blending of the PAH molecules they consist of. In addition, the MD

results obtained here are in contrast with Eq. 3 (orange line) proposed⁴² for soot using particle diameter, $d_p = 2.5$ nm (consistent with the size of cluster E, $d_g = 2r_g = 2.46$ nm), which indicates faster coalescence with increasing temperature. Equation 3 describes coalescence by viscous flow of material from the bulk to the neck region and does not account for structural characteristics of the coalescing clusters, such as aromatic-to-aliphatic ratio or C/H ratio, thus predicting faster coalescence at higher temperatures. Similar temperature-dependence is also predicted by coalescence due to surface diffusion (Eq. 2), resulting, however, to $\tau_c > 100$ ns (not shown here) for the cluster sizes and temperatures investigated here. Nonetheless, high temperatures promote the formation of more aromatic rings (as shown in Figs. 4a and c) that enhance the rigidity of incipient soot clusters, to slower or no coalescence.

Figure 6b shows the probability of coalescence, i.e. the clusters' probability to coalesce forming a dimer with $a/a_0 < 0.863$, for soot cluster pairs (B, B) (diamonds), (C, C) (triangles), (D, D) (circles) and (E, E) (squares) as function of temperature. For each combination of clusters and temperature, seven independent coalescence simulations were performed with random initial orientation. The coalescence probability is extracted from these seven coalescence simulations for each cluster size and temperature. At $T = 800$ K, all simulated soot clusters coalesce fully leading to round particles (e.g., Fig. 3a), while no bounce events are observed. As temperature increases, the fraction of soot clusters that coalesce decreases. At high temperatures, incipient soot particles typically exhibit higher aromatic-to-aliphatic C ratios (Fig. 2) indicating the formation of harder structures (stiff clusters) that are less prone to coalesce, leading to very low or zero probability of coalescence (Fig. 6b: $T \geq 1200$ K).

Figure 6

4. Conclusions

The formation mechanism of soot nuclei was investigated by reactive molecular dynamics (MD) simulations. The generated nascent soot particles are characterized in terms of their composition (C/H ratio, aromatic-to-aliphatic ratio), size and structural characteristics (number of 5-, 6- and 7-member rings, packing density). Nascent soot nanoparticles formed *ab initio* by nucleation and surface growth attain “atomic” fractal dimensions of 2.4 – 2.8 and C/H ratio of ~2.5. The clusters exhibit a core-shell structure consisting of an aromatic core and an aliphatic shell. Coalescence of soot clusters is investigated at various process temperatures and particle sizes. At low temperatures, particles are more prone to coalescence as they exhibit lower aromatic-to-aliphatic ratio and smaller C/H ratios.

Coalescence takes place due to reactions among the aliphatic chains at the particle surface. Large particles consisting of more than 760 atoms have smaller surface-to-volume ratio and aromatic-to-aliphatic ratio greater than 1, therefore, they are less likely to coalesce. The characteristic coalescence time is determined by monitoring the evolution of the surface area of the coalescing soot clusters and hardly changes as function of particle size for clusters consisting of 247 – 760 atoms. However, the coalescence rate depends on the cluster structure and composition, quantified by the aromatic-to-aliphatic carbon ratio, which, in turn, depends strongly on the particle size and the process temperature. Specifically, incipient soot clusters with aromatic-to-aliphatic carbon ratio smaller than 1, coalesce with characteristic coalescence time of the order of 0.1 ns, while no coalescence is observed for clusters with larger aromatic-to-aliphatic carbon ratios for the time scales investigated (i.e., up to 10 ns). The coalescence rate slows down slightly as the process temperature increases, in contrast to viscous flow or surface diffusion sintering mechanisms.

5. Acknowledgements

E.G. and A.S. acknowledge funding from the Melbourne School of Engineering through the 2020 Early Career Research Grant and from the Selby Scientific Foundation through the 2020 Selby Research Award. S.R. and K.M.M acknowledge funding support of Wallace Endowment Fund at Marquette University.

Supplementary Information

Figures showing the evolution of the composition (C/H ratio), particle size and shape (diameter, packing density and “atomic” fractal dimension) of incipient soot clusters during nucleation at 1500 K, as well as the normalized surface area at various temperatures and snapshots of soot clusters during coalescence.

6. References

1. Michelsen HA, Colket, M. B., Bengtsson, P. E., D’Anna, A., Desgroux, P., Haynes, B. S., Miller, H., Nathan, G. J, Pitsch, H., Wang, H. A Review of Terminology Used to Describe Soot Formation and Evolution under Combustion and Pyrolytic Conditions. *Acs Nano*. 2020;14(10):12470-12490.
2. Jacobsen NR, Pojana G, White P, et al. Genotoxicity, cytotoxicity, and reactive oxygen species induced by single-walled carbon nanotubes and C-60 fullerenes in the FE1-Muta (TM) mouse lung epithelial cells. *Environ Mol Mutagen*. Jul 2008;49(6):476-487.
3. Jerrett M, Burnett RT, Beckerman BS, et al. Spatial Analysis of Air Pollution and Mortality in California. *Am J Resp Crit Care*. Sep 1 2013;188(5):593-599.

4. Mahrt F, Marcolli C, David RO, et al. Ice nucleation abilities of soot particles determined with the Horizontal Ice Nucleation Chamber. *Atmos Chem Phys*. Sep 20 2018;18(18):13363-13392.
5. Jacobson MZ. Strong radiative heating due to the mixing state of black carbon in atmospheric aerosols. *Nature*. Feb 8 2001;409(6821):695-697.
6. Wegner K, Pratsinis SE. Scale-up of nanoparticle synthesis in diffusion flame reactors. *Chem Eng Sci*. Oct 2003;58(20):4581-4589.
7. Meierhofer F, Fritsching, U. Synthesis of Metal Oxide Nanoparticles in Flame Sprays: Review on Process Technology, Modeling, and Diagnostics. *Energ Fuel*. 2021;in press.
8. Schatz A, Grass RN, Stark WJ, Reiser O. TEMPO Supported on Magnetic C/Co-Nanoparticles: A Highly Active and Recyclable Organocatalyst. *Chem-Eur J*. 2008;14(27):8262-8266.
9. Shepelin NA, Sherrell PC, Goudeli E, et al. Printed recyclable and self-poled polymer piezoelectric generators through single-walled carbon nanotube templating. *Energ Environ Sci*. Mar 1 2020;13(3):868-883.
10. Sun YP, Zhou B, Lin Y, et al. Quantum-sized carbon dots for bright and colorful photoluminescence. *J Am Chem Soc*. Jun 21 2006;128(24):7756-7757.
11. Wang H. Formation of nascent soot and other condensed-phase materials in flames. *P Combust Inst*. 2011;33:41-67.
12. Balthasar A, Kraft M. A stochastic approach to calculate the particle size distribution function of soot particles in laminar premixed flames. *Combust Flame*. May 2003;133(3):289-298.
13. Wang BY, Mosbach S, Schmutzhard S, Shuai SJ, Huang YQ, Kraft M. Modelling soot formation from wall films in a gasoline direct injection engine using a detailed population balance model. *Appl Energ*. Feb 1 2016;163:154-166.
14. Mao Q, van Duin ACT, Luo KH. Formation of incipient soot particles from polycyclic aromatic hydrocarbons: A ReaxFF molecular dynamics study. *Carbon*. Sep 2017;121:380-388.
15. Johansson KO, Head-Gordon MP, Schrader PE, Wilson KR, Michelsen HA. Resonance-stabilized hydrocarbon-radical chain reactions may explain soot inception and growth. *Science*. Sep 7 2018;361(6406):997-+.
16. Totton TS, Chakrabarti D, Misquitta AJ, Sander M, Wales DJ, Kraft M. Modelling the internal structure of nascent soot particles. *Combust Flame*. May 2010;157(5):909-914.
17. Chung SH, Violi A. Peri-condensed aromatics with aliphatic chains as key intermediates for the nucleation of aromatic hydrocarbons. *P Combust Inst*. 2011;33:693-700.
18. Elvati P, Violi A. Thermodynamics of poly-aromatic hydrocarbon clustering and the effects of substituted aliphatic chains. *P Combust Inst*. 2013;34:1837-1843.
19. Mao Q, Ren YH, Luo KH, van Duin ACT. Dynamics and kinetics of reversible homo-molecular dimerization of polycyclic aromatic hydrocarbons. *J Chem Phys*. Dec 28 2017;147(24).
20. Yuan HL, Kong WJ, Liu FS, Chen DP. Study on soot nucleation and growth from PAHs and some reactive species at flame temperatures by ReaxFF molecular dynamics. *Chem Eng Sci*. Feb 23 2019;195:748-757.
21. Chen C, Jiang X. Molecular dynamics simulation of soot formation during diesel combustion with oxygenated fuel addition. *Phys Chem Chem Phys*. Sep 28 2020;22(36):20829-20836.
22. Richter H, Howard JB. Formation of polycyclic aromatic hydrocarbons and their growth to soot - a review of chemical reaction pathways. *Prog Energ Combust*. 2000;26(4-6):565-608.
23. Ono K, Dewa K, Matsukawa Y, et al. Experimental evidence for the sintering of primary soot particles. *J Aerosol Sci*. Mar 2017;105:1-9.
24. Botero ML, Eaves N, Dreyer JAH, et al. Experimental and numerical study of the evolution of soot primary particles in a diffusion flame. *P Combust Inst*. 2019;37(2):2047-2055.
25. Goudeli E, Pratsinis SE. Crystallinity dynamics of gold nanoparticles during sintering or coalescence. *Aiche J*. Feb 2016;62(2):589-598.
26. Hou D, Chu, Q., Chen, D., Pascazio, L., Kraft, M., & You, X. Atomic insights into the sintering process of polycyclic aromatic hydrocarbon clusters. *P Combust Inst*. 2020.

27. Buesser B, Grohn AJ, Pratsinis SE. Sintering Rate and Mechanism of TiO₂ Nanoparticles by Molecular Dynamics. *J Phys Chem C*. Jun 9 2011;115(22):11030-11035.
28. Zhang CY, Zhang C, Ma Y, Xue XG. Imaging the C black formation by acetylene pyrolysis with molecular reactive force field simulations. *Phys Chem Chem Phys*. 2015;17(17):11469-11480.
29. Roy SP. Aerosol-dynamics-based soot modeling of flames. PhD thesis, *The Pennsylvania State University*. 2014.
30. Castro-Marciano F, Kamat AM, Russo MF, van Duin ACT, Mathews JP. Combustion of an Illinois No. 6 coal char simulated using an atomistic char representation and the ReaxFF reactive force field. *Combust Flame*. Mar 2012;159(3):1272-1285.
31. Chenoweth K, van Duin ACT, Goddard WA. ReaxFF reactive force field for molecular dynamics simulations of hydrocarbon oxidation. *J Phys Chem A*. Feb 7 2008;112(5):1040-1053.
32. Swope WC, Andersen HC, Berens PH, Wilson KR. A Computer-Simulation Method for the Calculation of Equilibrium-Constants for the Formation of Physical Clusters of Molecules - Application to Small Water Clusters. *J Chem Phys*. 1982;76(1):637-649.
33. Chenoweth K, van Duin ACT, Dasgupta S, Goddard WA. Initiation Mechanisms and Kinetics of Pyrolysis and Combustion of JP-10 Hydrocarbon Jet Fuel. *J Phys Chem A*. Mar 5 2009;113(9):1740-1746.
34. Evans DJ, Holian BL. The Nose-Hoover Thermostat. *J Chem Phys*. 1985;83(8):4069-4074.
35. Plimpton S. Fast Parallel Algorithms for Short-Range Molecular-Dynamics. *J Comput Phys*. Mar 1 1995;117(1):1-19.
36. Buesser B, Grohn AJ, Pratsinis SE. Sintering Rate and Mechanism of TiO₂ Nanoparticles by Molecular Dynamics. *J Phys Chem C Nanomater Interfaces*. Jun 9 2011;115(22):11030-11035.
37. Sanner MF, Olson AJ, Spehner JC. Reduced surface: An efficient way to compute molecular surfaces. *Biopolymers*. Mar 1996;38(3):305-320.
38. Brunauer S, Emmett PH, Teller E. Adsorption of gases in multimolecular layers. *J Am Chem Soc*. Jan-Jun 1938;60:309-319.
39. Kobata A, Kusakabe K, Morooka S. Growth and Transformation of TiO₂ Crystallites in Aerosol Reactor. *Aiche J*. Mar 1991;37(3):347-359.
40. Koch W, Friedlander SK. The Effect of Particle Coalescence on the Surface-Area of a Coagulating Aerosol. *J Colloid Interf Sci*. Dec 1990;140(2):419-427.
41. Veshkini A, Dworkin SB, Thomson MJ. Understanding soot particle size evolution in laminar ethylene/air diffusion flames using novel soot coalescence models. *Combust Theor Model*. 2016;20(4):707-734.
42. Chen DP, Zainuddin Z, Yapp E, Akroyd J, Mosbach S, Kraft M. A fully coupled simulation of PAH and soot growth with a population balance model. *P Combust Inst*. 2013;34:1827-1835.
43. Tsantilis S, Briesen H, Pratsinis SE. Sintering time for silica particle growth. *Aerosol Sci Tech*. Mar 2001;34(3):237-246.
44. Khaled Mosharraf Mukut, & Somesh Roy. (2020, November 21). kmmukut/RingDetection: RingDetection (Version v1.01). Zenodo. <http://doi.org/10.5281/zenodo.4283067>
45. Kim Y, Kim WY. Universal Structure Conversion Method for Organic Molecules: From Atomic Connectivity to Three-Dimensional Geometry. *Bulletin of the Korean Chemical Society*. 2015;36(7):1769-1777.
46. Cormen TH. *Introduction to algorithms*. 3rd ed MIT Press, Cambridge, MA (2009).
47. Hagberg A SD, Swart P. Exploring Network Structure, Dynamics, and Function using NetworkX. *Proceedings of the 7th Python in Science Conference (SciPy2008)*. Pasadena, CA USA (2008):11-15.
48. Johnson D. Finding all the elementary circuits of a directed graph. *SIAM Journal on Computing*. 1975;4(1):77-84.
49. JB K. On the shortest spanning subtree of a graph and the traveling salesman problem. *Proceedings of the American Mathematical Society*. 1956;7(1):48-50.
50. Kozen D. Depth-First and Breadth-First Search. In: *The Design and Analysis of Algorithms*. Texts and Monographs in Computer Science. Springer, New York, NY. 1992.

51. Weininger D. Smiles, a Chemical Language and Information-System .1. Introduction to Methodology and Encoding Rules. *J Chem Inf Comp Sci*. Feb 1988;28(1):31-36.
52. Landrum G. RDKit: Open-source cheminformatics. <http://www.rdkit.org>. (last accessed November 20, 2020).
53. Abid AD, Heinz N, Tolmacheff ED, Phares DJ, Campbell CS, Wang H. On evolution of particle size distribution functions of incipient soot in premixed ethylene-oxygen-argon flames. *Combust Flame*. Sep 2008;154(4):775-788.
54. Russo C, Tregrossi A, Ciajolo A. Dehydrogenation and growth of soot in premixed flames. *P Combust Inst*. 2015;35:1803-1809.
55. Jacobson RS, Korte AR, Vertes A, Miller JH. The Molecular Composition of Soot. *Angew Chem Int Edit*. Mar 9 2020;59(11):4484-4490.
56. Commodo M, Kaiser K, De Falco G, et al. On the early stages of soot formation: Molecular structure elucidation by high-resolution atomic force microscopy. *Combust Flame*. Jul 2019;205:154-164.
57. Siegmann K, Sattler K. Formation mechanism for polycyclic aromatic hydrocarbons in methane flames. *J Chem Phys*. Jan 8 2000;112(2):698-709.
58. Mandelbrot BB. The Fractals Book. *Observatory*. 1982;102(1049):151-151.
59. Kelesidis GA, Pratsinis SE. Soot light absorption and refractive index during agglomeration and surface growth. *P Combust Inst*. 2019;37(1):1177-1184.
60. Kelesidis GA, Goudeli E, Pratsinis SE. Flame synthesis of functional nanostructured materials and devices: Surface growth and aggregation. *P Combust Inst*. 2017;36(1):29-50.
61. Mosbach S, Celnik MS, Raj A, et al. Towards a detailed soot model for internal combustion engines. *Combust Flame*. Jun 2009;156(6):1156-1165.
62. Dandajeh HA, Ladommatos N, Hellier P, Eveleigh A. Effects of unsaturation of C-2 and C-3 hydrocarbons on the formation of PAHs and on the toxicity of soot particles. *Fuel*. Apr 15 2017;194:306-320.
63. Oktem B, Tolocka MP, Zhao B, Wang H, Johnston MV. Chemical species associated with the early stage of soot growth in a laminar premixed ethylene-oxygen-argon flame. *Combust Flame*. Sep 2005;142(4):364-373.
64. Cain JP, Camacho J, Phares DJ, Wang H, Laskin A. Evidence of aliphatics in nascent soot particles in premixed ethylene flames. *P Combust Inst*. 2011;33:533-540.
65. Frenklach M, Mebel AM. On the mechanism of soot nucleation. *Phys Chem Chem Phys*. Mar 7 2020;22(9):5314-5331.
66. Arcidiacono S, Bieri NR, Poulikakos D, Grigoropoulos CP. On the coalescence of gold nanoparticles. *Int J Multiphas Flow*. Jul-Aug 2004;30(7-8):979-994.
67. Goudeli E, Pratsinis SE. Surface Composition and Crystallinity of Coalescing Silver-Gold Nanoparticles. *Acs Nano*. Nov 2017;11(11):11653-11660.

Figures

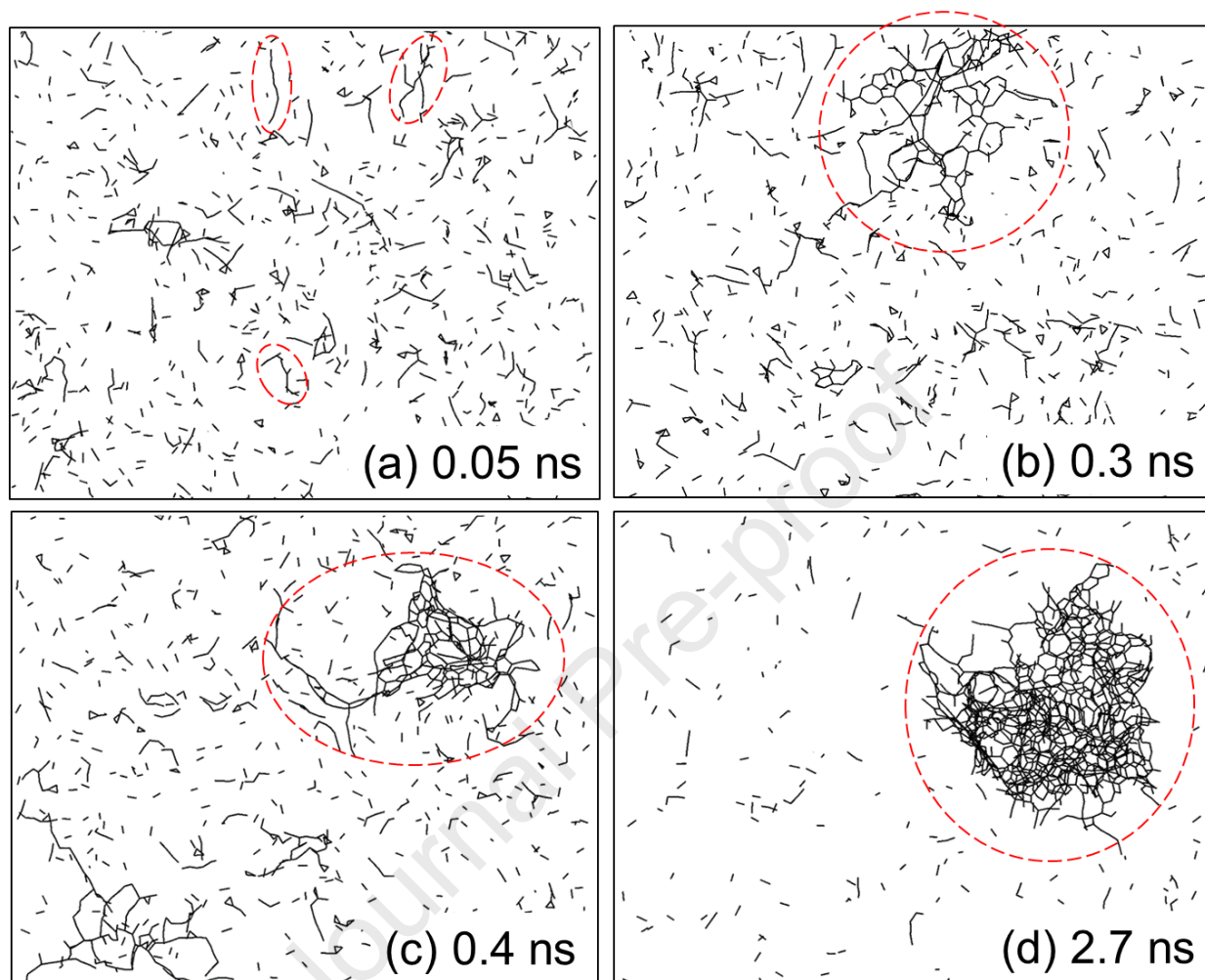


Figure 1. Snapshots of the carbonaceous species (black lines correspond to carbon aliphatic and aromatic chains; hydrogen atoms are omitted) formed by acetylene collisions at 1500 K after (a) 0.05, (b) 0.3, (c) 0.4 and (d) 2.7 ns. The first nuclei (red-circled molecules) are formed by chain elongation (0.01 ns), cyclization with the formation of branched PAHs (0.3 ns) and sticking to form nascent soot clusters (0.4 ns) which grow further by condensation of small free molecules on their surface (2.7 ns).

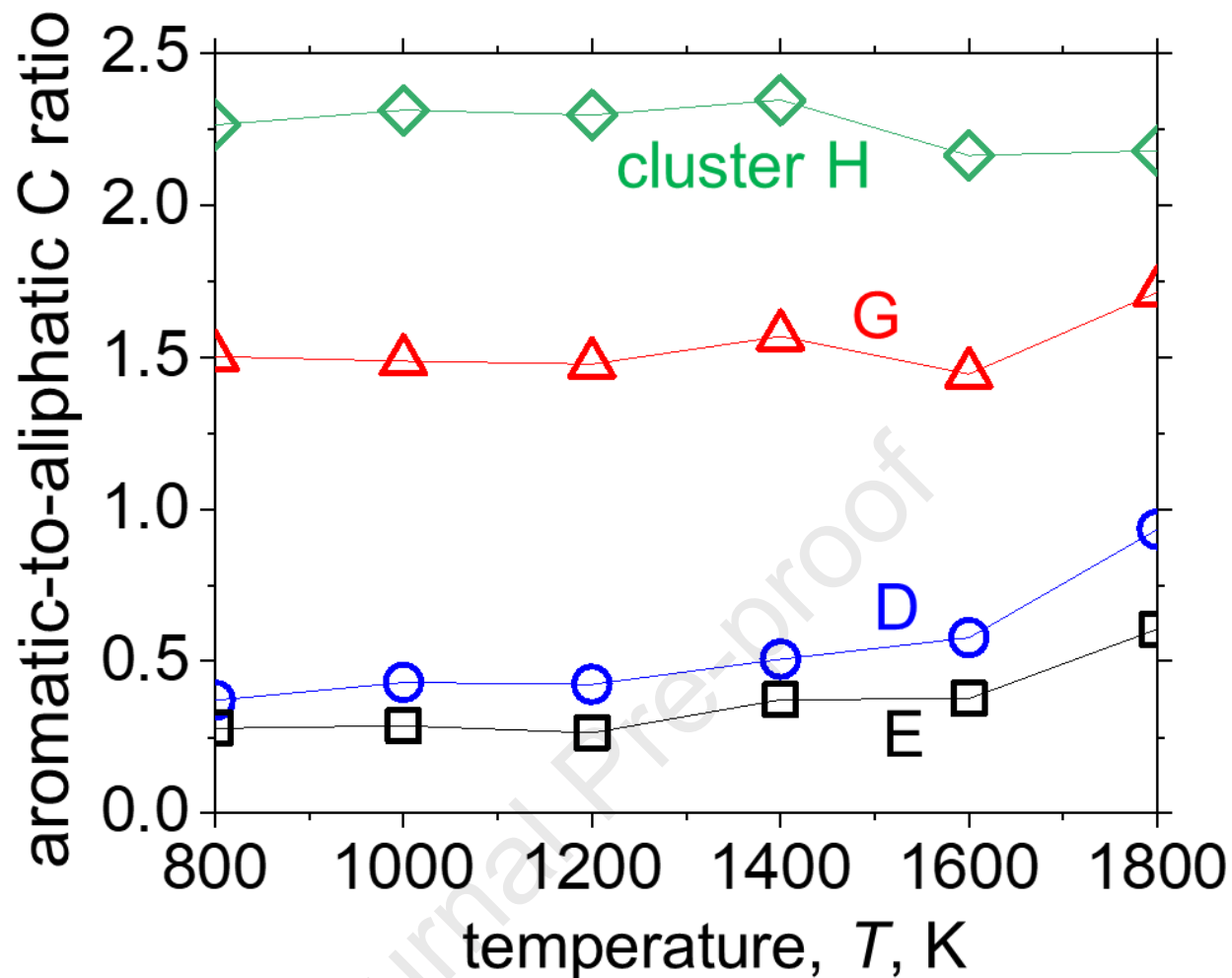


Figure 2. The aromatic-to-aliphatic carbon ratio is shown as function of the temperature for single incipient soot particles consisting of 449 (cluster D, circles), 760 (cluster E, squares), 1769 (cluster G, triangles) and 1927 atoms (cluster H, diamonds) after they are extracted during nucleation at 1500 K (Fig. 1) and simulated isothermally at 800 – 1800 K. The number of atoms represent the total number of atoms for the cluster when they were extracted from the nucleation simulation (at 1500 K). The temperatures indicate the temperature at which these clusters restructured (see Sec 2.2) before coalescence.

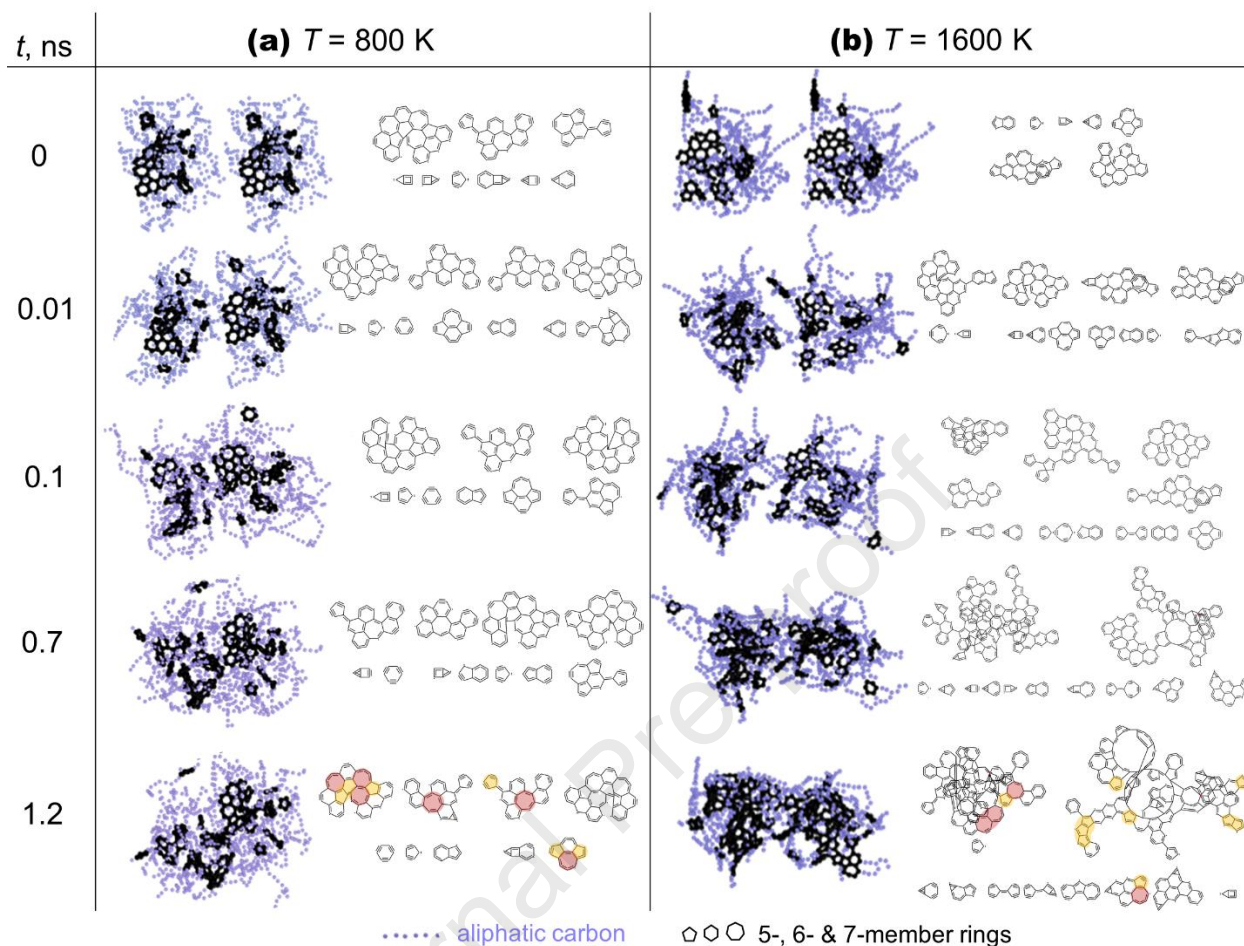


Figure 3. 3D snapshots (left columns) and chemical structure (right columns) of pairs of incipient soot clusters, corresponding to cluster E in Table 2, with initial radius of gyration, $r_g = 1.23 \text{ nm}$, coalescing at (a) 800 K and (b) 1600 K. Only C atoms are shown, with blue dots indicating aliphatic C atoms and black rings depicting 5-, 6- and 7-member rings. The 5- and 7-membered rings are marked respectively with yellow and red highlights at $t = 1.2 \text{ ns}$.

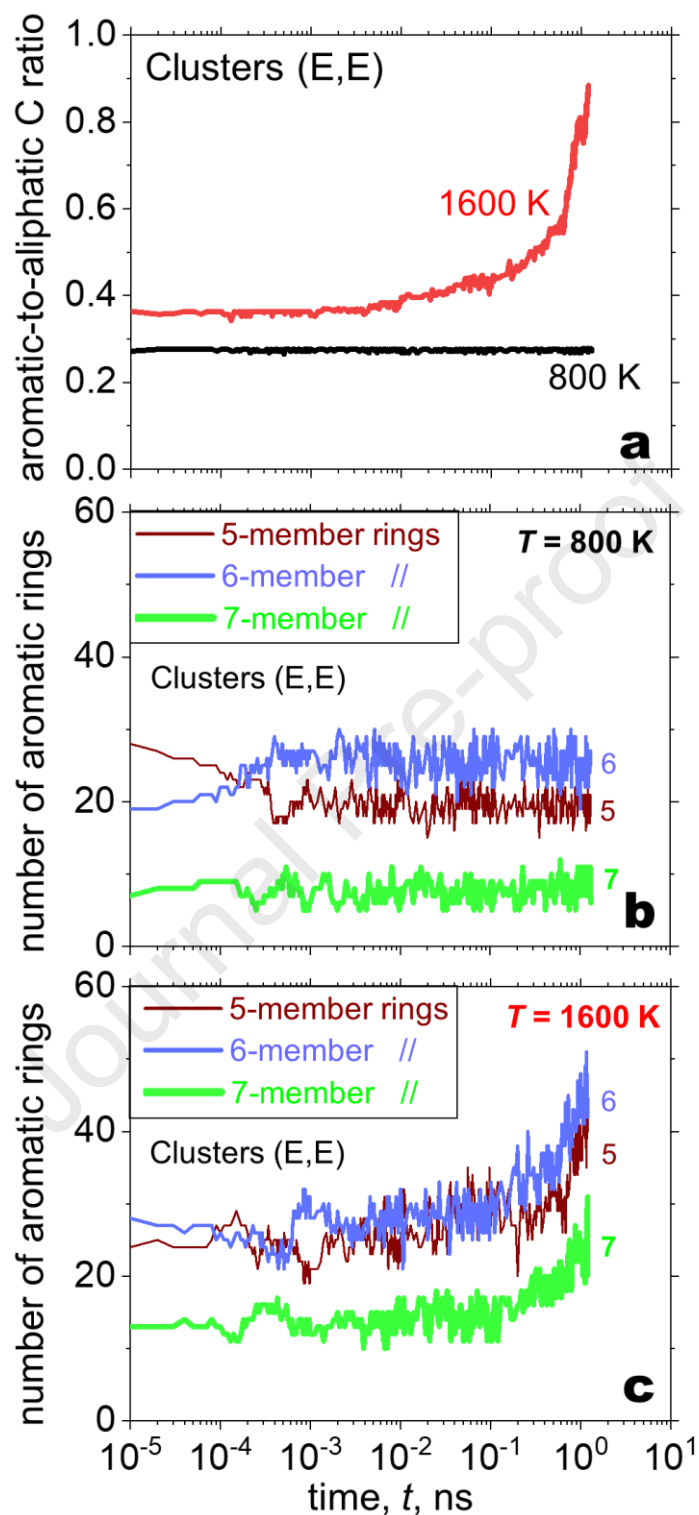


Figure 4. (a) The temporal evolution of the aromatic-to-aliphatic carbon ratio of coalescing soot clusters (E, E) at 800 K (black line) and 1600 K (red line). At high temperatures the aromatic-to-aliphatic carbon ratio increases during coalescence due to aromatization reactions, while at low temperatures (800 K) no aromatization is observed throughout coalescence for up to 1 ns investigated here. The temporal evolution of the number of 5- (brown lines), 6- (blue lines) and 7-member rings (green lines) of coalescing clusters (E, E) is shown at (b) 800 K and (c) 1600 K.

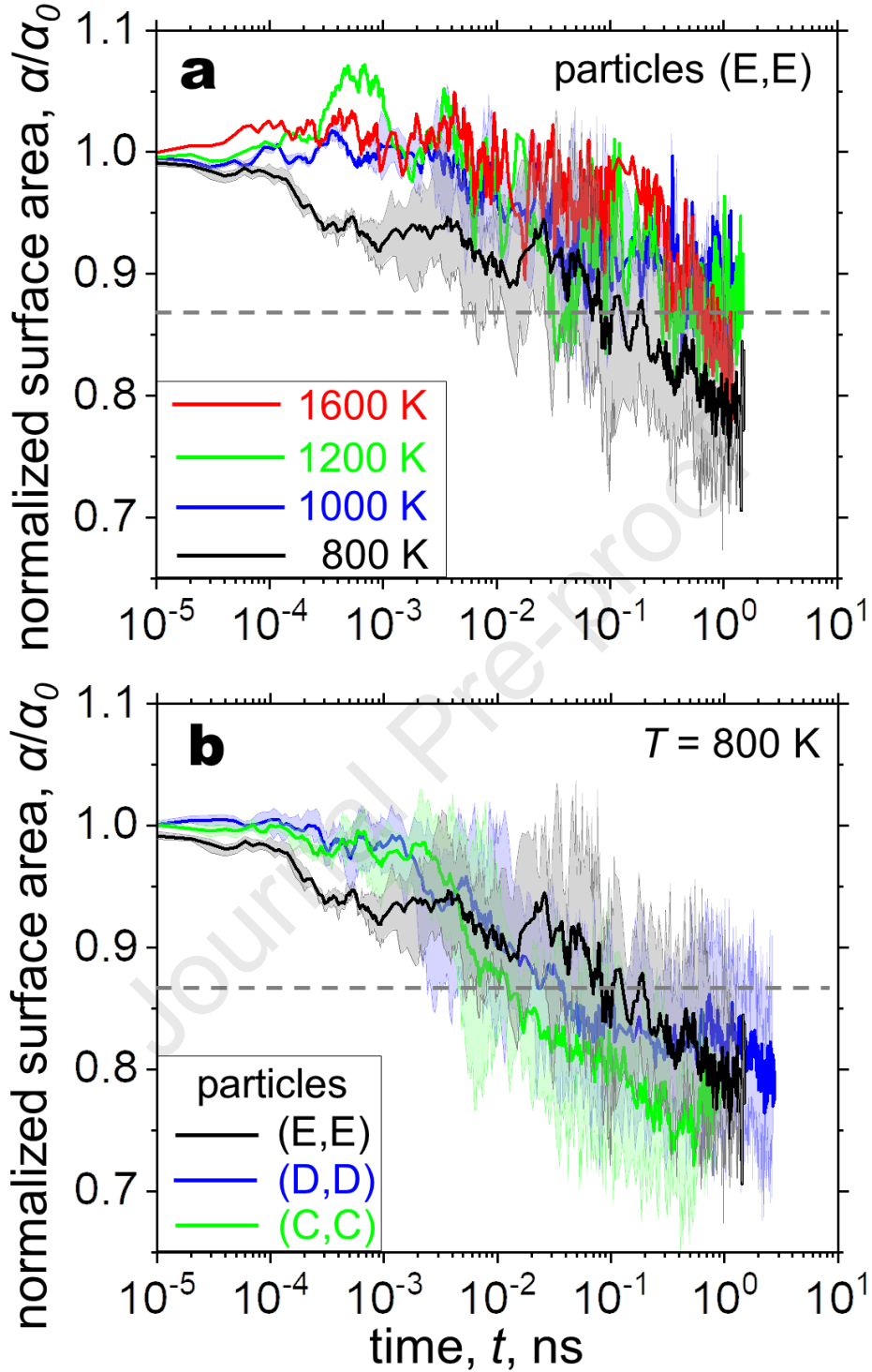


Figure 5. (a) Temporal evolution of the normalized surface area, a/a_0 , during coalescence of soot clusters with initial $d_g = 2.5$ nm at 1600 K (red line), 1200 K (green lines), 1000 K (blue lines) and 800 K (black lines). (b) Temporal evolution of the normalized surface area, a/a_0 , during coalescence of soot clusters with initial $d_g = 2.5$ (black line), 1.88 (blue line) and 1.9 nm (green line) at 800 K. The lightly colored shaded areas represent the variability of multiple coalescence simulations. The broken horizontal line at $a/a_0 = 0.863$ indicated the characteristic coalescence time, τ_c , which corresponds to the time required for the free surface area to decrease by 67%³⁶.

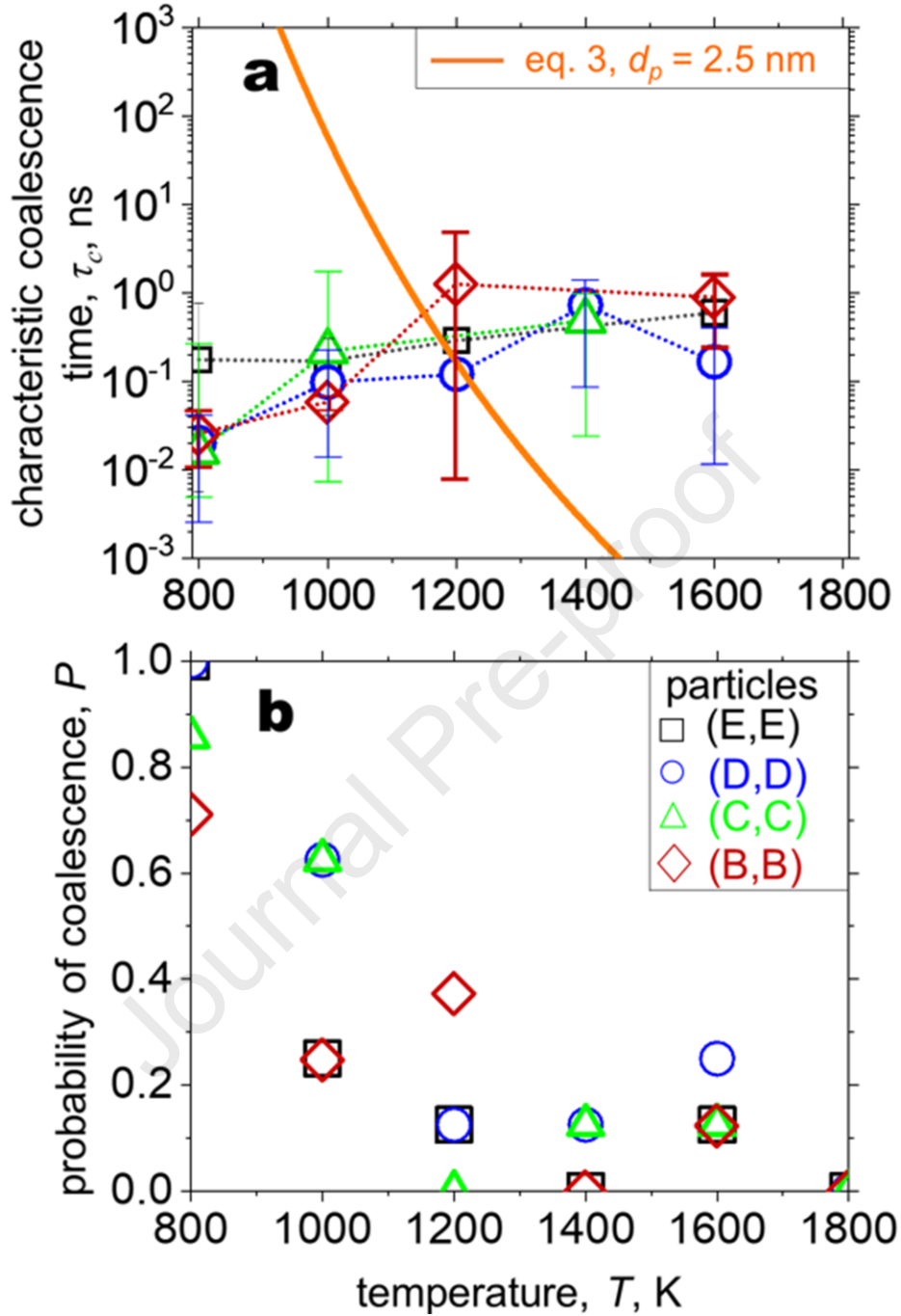


Figure 6. (a) MD-obtained characteristic coalescence time, τ_c (symbols), for coalescing incipient soot clusters (B, B) (diamonds), (C, C) (triangles), (D, D) (circles) and (E, E) (squares) as function of the process temperature, T . Increasing temperature results in slightly slower coalescence rates (increasing τ_c). The MD results contrast with a viscous flow sintering rate (orange line⁴²) which indicates faster coalescence with increasing temperature. (b) The probability of coalescence indicating the probability of pair soot clusters (B, B) (diamonds), (C, C) (triangles), (D, D) (circles) and (E, E) (squares) to coalesce forming a dimer with $a/a_0 < 0.863$ is shown as function of temperature.

Table 1. Exemplary snapshots of incipient soot clusters obtained during nucleation and surface growth at 1500 K (Fig. 1). The number of atoms, radius of gyration, r_g , aromatic-to-aliphatic C ratio and number of 5-, 6- and 7-member rings are listed for each particle.


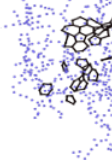
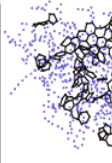
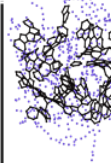
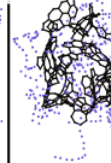
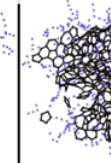
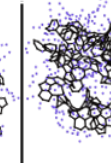
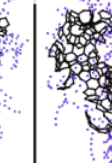
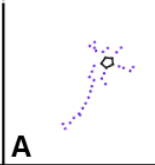
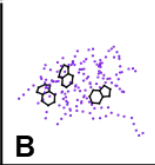
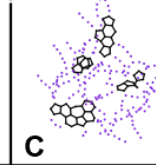
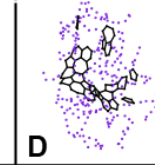
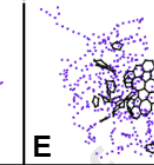
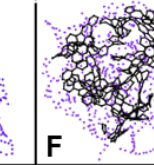
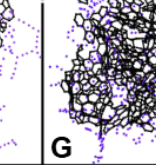
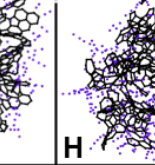
								
time, ns	0.25	0.5	0.75	1	1.25	1.5	1.75	2
no. of atoms	178	851	1367	1450	1478	1754	1782	1800
r_g , nm	0.834	1.32	1.36	1.37	1.36	1.43	1.41	1.43
aromatic/aliphatic C ratio	0.223	0.242	0.412	0.838	1.28	1.27	1.32	1.46
5-member rings	2	6	19	28	31	47	38	41
6-member rings	1	8	29	53	81	76	76	85
7-member rings	2	12	12	23	22	32	41	40

Table 2. Snapshots of incipient soot clusters A – H, obtained during nucleation and surface growth at 1500 K (Fig. 1), are selected for coalescence simulations. The number of atoms, radius of gyration, r_g , aromatic-to-aliphatic C ratio and number of 5-, 6- and 7-member rings are listed for each particle. Clusters A – H are further simulated in *NVT* at various temperatures and are replicated to coalesce in vacuum.

								
	A	B	C	D	E	F	G	H
time, ns	0.168	0.32	0.35	0.39	0.47	0.99	2	5.4
no. of atoms	50	247	348	449	760	1404	1769	1927
r_g , nm	0.63	0.81	1.03	0.99	1.23	1.35	1.39	1.39
aromatic/aliphatic C ratio	0.17	0.19	0.38	0.37	0.28	0.89	1.5	2.26
5-member rings	1	2	8	9	14	30	37	66
6-member rings	0	5	8	10	11	55	89	110
7-member rings	0	0	2	4	4	23	39	34

Declaration of interests

The authors declare that they have no known competing financial interests or personal relationships that could have appeared to influence the work reported in this paper.

The authors declare the following financial interests/personal relationships which may be considered as potential competing interests:

Journal Pre-proof